Received: 25 September 2018 | Revised: 14 January 2019 | Accepted: 22 January 2019

DOI: 10.1002/bit.26935

ARTICLE

WILEY BIOTECHNOLOGY AND BIOENGINEERING

Process monitoring of virus-like particle reassembly by diafiltration with UV/Vis spectroscopy and light scattering

Matthias Rüdt* | Philipp Vormittag* | Nils Hillebrandt | Jürgen Hubbuch

Institute of Engineering in Life Sciences, Section IV: Biomolecular Separation Engineering, Karlsruhe Institute of Technology (KIT), Karlsruhe, Germany

Correspondence
Jürgen Hubbuch, Fritz-Haber-Weg 2, 76131 Karlsruhe, Germany.
Email: juergen.hubbuch@kit.edu

Funding information
Deutsche Forschungsgemeinschaft, Grant/Award Number: 273937032

Abstract

Virus-like particles (VLPs) have shown great potential as biopharmaceuticals in the market and in clinics. Nonenveloped, in vivo assembled VLPs are typically disassembled and reassembled in vitro to improve particle stability, homogeneity, and immunogenicity. At the industrial scale, cross-flow filtration (CFF) is the method of choice for performing reassembly by diafiltration. Here, we developed an experimental CFF setup with an on-line measurement loop for the implementation of process analytical technology (PAT). The measurement loop included an ultraviolet and visible (UV/Vis) spectrometer as well as a light scattering photometer. These sensors allowed for monitoring protein concentration, protein tertiary structure, and protein quaternary structure. The experimental setup was tested with three Hepatitis B core Antigen (HBcAg) variants. With each variant, three reassembly processes were performed at different transmembrane pressures (TMPs). While light scattering provided information on the assembly progress, UV/Vis allowed for monitoring the protein concentration and the rate of VLP assembly based on the microenvironment of Tyrosine-132. VLP formation was verified by off-line dynamic light scattering (DLS) and transmission electron microscopy (TEM). Furthermore, the experimental results provided evidence of aggregate-related assembly inhibition and showed that off-line size-exclusion chromatography does not provide a complete picture of the particle content. Finally, a Partial-Least Squares (PLS) model was calibrated to predict VLP concentrations in the process solution. Q^2 values of 0.947–0.984 were reached for the three HBcAg variants. In summary, the proposed experimental setup provides a powerful platform for developing and monitoring VLP reassembly steps by CFF.

KEYWORDS
cross-flow filtration, downstream processing, process analytical technology, self-assembly, spectroscopy, virus-like particles

1 | INTRODUCTION

Virus-like particles (VLPs) are biopharmaceuticals with potential applications against various diseases such as viral and bacterial infections, cancer, Alzheimer's disease, and autoimmune disorders (Bachmann & Whitehead, 2013; Klamp et al., 2011; Kushnir, Streatfield, & Yusibov, 2012; Lua et al., 2014; Middelberg et al., 2011). They are generally designed to trigger an immune response by presenting antigens on their surface. These antigens are either part of the native viral capsid or introduced artificially. Chimeric VLPs

*Rüdt and Vormittag have contributed equally.

were, for example, constructed based on hepatitis B core antigen (HBcAg) (Arora, Tyagi, Swaminathan, & Khanna, 2012; Klamp et al., 2011; Whitacre, Lee, & Milich, 2009), hepatitis B surface antigen (HBsAg) (Kaslow & Biernaux, 2015), GH1-Qβ (Low et al., 2014), and murine polyomavirus VP1 (MuPyVP1) (Middelberg et al., 2011). VLPs are resilient to most environmental stresses, have great potential to be produced inexpensively, and efficiently elicit potent immune responses due to their repetitive and particulate structure (Chuan, Wibowo, Lua, & Middelberg, 2014; Kumru et al., 2014).

Similar to viruses, VLPs are assemblies of one or several types of capsid proteins forming a higher order structure (Lua et al., 2014). VLPs are expressed in genetically modified host organisms (Kushnir et al., 2012; Lua et al., 2014; Vicente, Roldão, Peixoto, Carrondo, & Alves, 2011). Subsequent production-scale purification most frequently consists of precipitation, chromatography, and ultrafiltration/diafiltration (UF/DF) (Ladd Effio, & Hubbuch, 2015). In vivo self assembled, nonenveloped VLPs are often disassembled and subsequently reassembled to remove impurities from within the capsid (Link et al., 2012; Ren, Wong, & Lim, 2006). Disassembling and reassembling also leads to increased structural homogeneity, improved overall stability, and enhanced antigenicity (Mach et al., 2006; Zhao, Allen et al., 2012, Zhao, Modis et al., 2012). An overview of a typical VLP production process is given in Figure 1.

Generally, a change in the quaternary structure of VLPs is induced by altering their physicochemical environment, i.e., the ionic strength of the protein solution, the pH, or the concentration of a reducing agent (Zhao, Allen et al., 2012). At lab scale, dialysis is the most common method for buffer exchanges (Mach et al., 2006). Dialysis has, however, some drawbacks such as long processing times and significant buffer consumption (Kurnik et al., 1995). In preparative downstream processes, cross-flow filtration (CFF) is more popular because of its simple scalability, reduced buffer consumption, and reduced processing time (Jornitz, Jornitz, & Meltzer, 2008; Kurnik et al., 1995). CFF has been successfully applied to VLPs for capture, buffer exchange, and concentration (Russell et al., 2007; Vicente et al., 2011, 2014). Compared with dialysis and batch diafiltration, assembly of VLPs by constant volume diafiltration was shown to increase VLP yield (Liew, Chuan, & Middelberg, 2012). Despite the many advantages, CFF may also cause problems due to protein-membrane interaction (Hanemaaijer, Robbertsen, van den Boomgaard, & Gunnink, 1989; Ko, Pellegrino, Nassimbene, & Marko, 1993), which was observed to impact process performance (Peixoto, Sousa, Silva, Carrondo, & Alves, 2007). To reduce these problems, CFF process time has to be minimized while maximizing the process efficiency.

Process analytical technology (PAT; Bakeev, 2010; Roch & Mandenius, 2016; Rüdt, Briskot, & Hubbuch, 2017) is thus of interest to monitor the assembly progress. Protein concentration measurements allow detecting protein adsorption to the membrane. Particle size measurements provide information on the assembly progress of the capsid proteins into VLPs. Previous publications have also reported effects of the VLP tertiary structure on ultraviolet and visible (UV/Vis) and fluorescence absorption spectra (Ausar, Foubert, Hudson, Vedvick, & Middaugh, 2006; Fang et al., 2016; Hanslip, Zaccai, Middelberg, & Falconer, 2006; Hu et al., 2011; Rajendar et al., 2013). Following a systematic approach to process monitoring, a combination of PAT sensors should be chosen which allows monitoring protein concentration, protein tertiary structure, and protein size.

In this study, we developed a CFF setup consisting of a commercial lab scale CFF device with a custom-made on-line measurement loop for process analytical instrumentation. The on-line measurement loop included a light scattering photometer (dynamic light scattering [DLS] and static light scattering [SLS]) and a UV/Vis absorption spectrometer. DLS allowed for monitoring the mean hydrodynamic diameter of particles. SLS outputs an aggregated scattered light intensity influenced by the particle concentrations and the diameters. Finally, UV/Vis spectroscopy provided information on the protein concentration and on changes in the tertiary structure by second derivative spectroscopy (Jiskoot and Crommelin, 2005). The usefulness of the custom-made setup was

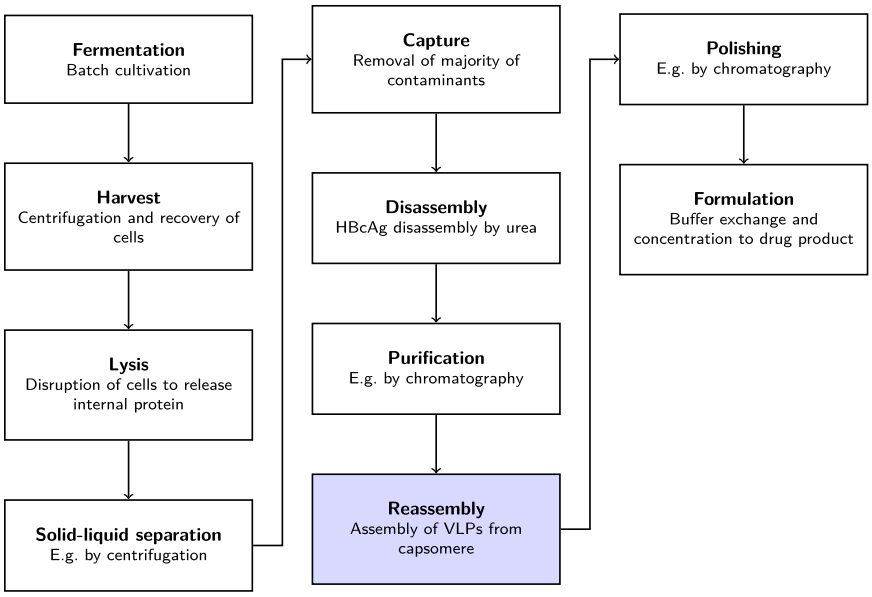

FIGURE 1 Illustration of a typical VLP production process. The downstream processing train may consist of eight or more unit operations. The unit operation investigated here—the VLP reassembly—is marked in blue. VLP: virus-like particle [Color figure can be viewed at wileyonlinelibrary.com]

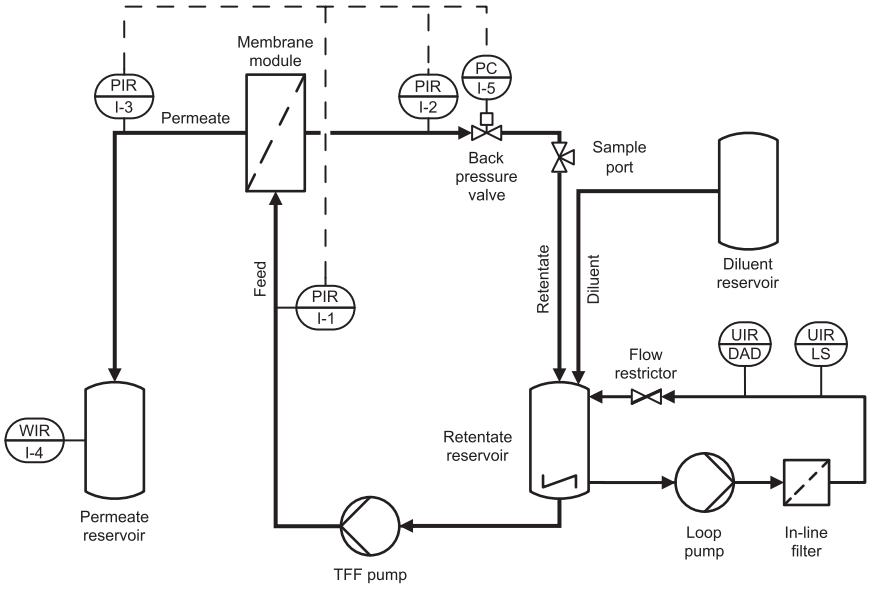

FIGURE 2 Piping and instrumentation diagram of the experimental setup. At the bottom right, the on-line measurement loop is shown. The remaining piping is required for the CFF. All sensors are connected to a computer for capturing the data centrally. Electronic communication lines are indicated by dashed lines. I-5 is a pinch valve actuated by a closed loop controller for the TMP. C: control; CFF: cross-flow filtration; DAD: diode array detector; I: indicate; LS: light scattering; P: pressure; R: record; TMP: transmembrane pressure; U: multivariable; W: weight

tested for monitoring the reassembly of three different chimeric HBcAg variants at three different transmembrane pressures (TMPs).

2 | MATERIALS AND METHODS

2.1 | Experimental setup

A custom-made setup was developed for the CFF experiments. Figure 2 shows the setup as a piping and instrumentation diagram (P&ID). A KrosFlo KRIIi CFF unit with a modified polyethersulfone (mPES) hollow fiber membrane module (10 kDa cutoff, 13 cm^2 membrane area) and a 50 ml conical tube retentate reservoir (Spectrum Labs, Rancho Dominguez, US-CA) made up the core of the CFF unit. A Topolino Magnetic Stirrer (IKA Werke, Staufen im Breisgau, DE) ensured homogeneous mixing of the retentate reservoir. A T-piece with injection plug (Fresenius Kabi, Bad Homburg, DE) was inserted into the retentate line as sample port to draw liquid for off-line analytics. The retentate reservoir was modified with two additional polyether ether ketone (PEEK) capillaries to supply the on-line measurement loop with liquid from the process.

In the direction of flow, the on-line measurement loop consisted of a Gilson Minipuls 3 peristaltic pump, a 0.7 μm particle retention Minisart glass fiber syringe filter (Sartorius Stedim Biotech, Göttingen, DE), a Zetasizer Nano ZSP photometer (Malvern Instruments, Malvern, UK) with a 10-mm pathlength flow cell (Hellma Analytics, Müllheim, DE), an Ultimate Diode Array Detector 3000 (DAD-3000; Dionex Corporation, Sunnyvale, US-CA) with a 0.4-mm pathlength flow cell, and a FR-902 flow restrictor (GE Healthcare, Chalfont St Giles, UK). The pump of the on-line measurement loop was controlled via a NI USB-6008 data acquisition device (National Instruments, Austin, US-TX).

2.2 | Proteins, chemicals, and buffers

Three chimeric HBcAg constructs, i.e., VLP A, B, and C provided by BioNTech Protein Therapeutics GmbH (Mainz, DE), were used in this study. The HBcAg variants were recombinantly modified in the major immunodominant region (MIR) to display three different peptides on their surfaces (see also Figure 3). All variants were present as homodimer stock solutions in disassembly buffer (3.5 M urea, 50 mM Tris(hydroxymethyl)-aminomethane, pH 9.0) as obtained after purification (see also Figure 1). Protein concentration calculations were based on extinction coefficients derived from the primary structure as provided by the ProtParam tool (Gasteiger et al., 2005) of the Swiss Institute of Bioinformatics (Lausanne, CH). The purity of the stock solutions was characterized by reversed-phase chromatography based on the absorbance at 280 nm as described in the Supporting Information Material B. Immediately before each experiment, stock solutions were diluted with disassembly buffer to a protein concentration of 1 g/L (by Ultraviolet absorbance at 280 nm) and filtered through a 0.2 μm PES 110 filter (VWR International, Radnor, US-PA). The reassembly buffer was a high-salt buffer at pH 7.0.

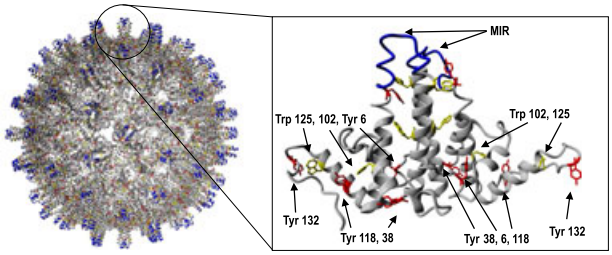

FIGURE 3 An assembled HBcAg VLP is shown on the left side (PDB ID 1QGT, (Wynne et al., 1999). The right side shows a cartoon of a single homodimer (adapted from PDB ID 4BMG, (Alexander et al., 2013). The tryptophan (Trp) and tyrosine (Tyr) side chains are depicted as sticks and colored in yellow and red, respectively. Tyr and Trp side chains located in the base of the molecule are numbered. These residues undergo a change of hydrophobicity in their environment during assembly. The MIR loop, whereto the foreign epitope is inserted, is shown in blue. HBcAg: hepatitis B core antigen; MIR: major immunodominant region; VLP: virus-like particle [Color figure can be viewed at wileyonlinelibrary.com]

For size-exclusion chromatography (SEC), 50 mM of potassium phosphate at pH 7.0 was used as running buffer. If not mentioned otherwise, chemicals were purchased from Merck KGaA (Darmstadt, DE). All buffers and solutions were prepared with ultrapure water (arium pro UV; Sartorius Stedim Biotech) and filtered through a 0.2 μm pore size Supor filter (Pall, Port Washington, US-NY) immediately before each experiment.

2.3 | VLP reassembly monitoring

The CFF unit and the measurement loop were filled with ultrapure water for pre-experimental preparation. The lamps of the DAD were turned on at least 1 hr before starting the experiments. At the end of the equilibration phase, the absorbance signal was zeroed in ultrapure water. Subsequently, the CFF unit and the measurement loop were first flushed with disassembly buffer and then changed into 25 ml of protein solution. The CFF pump was set to 70 ml/min corresponding to a shear rate of approximately 6000 s^{-1} in the hollow fibers. The measurement loop pump 1 ml/min and data acquisition were started.

After 5 min, constant TMP diafiltration was initiated by applying a TMP of 0.25, 0.5, or 1 bar with reassembly buffer as diluent. 0.4 ml samples were taken every 0.5 diafiltration volumes (DVs) via the sample port. Experiments were stopped after 3 DV except for VLP C for which the runs had to be terminated early due to membrane clogging. After each run, the CFF membrane was cleaned with ultrapure water, a 0.1 M of sodium hydroxide solution, and a 15 vol% of ethanol solution.

2.4 | Off-line sample analysis

For SEC analysis, samples were centrifuged (Centrifuge 5810R; Eppendorf, Hamburg, DE) at 3220 rcf for 5 min to settle large particles. The supernatant was analyzed with a Sepax SRT SEC-1000 column (Sepax Technologies, Newark, US-NJ) on an Ultimate 3000 RS ultra high performance liquid chromatography (UHPLC) system consisting of a Pump HPG-3400RS, an Autosampler WPS-3000TFC, a Column Compartment TCC-3000RS, and a Diode Array Detector DAD-3000 controlled by Chromeleon version 6.8 SR15 (Thermo Fisher Scientific, Waltham, US-MA). The run duration was 7 min with a flow rate of 0.8 ml/min and SEC buffer as a mobile phase. Twenty microlitre was injected for each analysis. Samples were analyzed in triplicates.

Off-line DLS analysis was performed using a sample volume of 45 μl in a 3x3 mm quartz cuvette (Hellma Analytics, Müllheim, DE) and the same DLS photometer as mentioned above. Unfiltered samples were measured three times, each measurement consisting of 12–14 10 s runs at 25°C, and 173°C backscatter. Lower and upper limits for data processing were 1 nm and 6000 nm, respectively. The measurements were compared based on the VLP peak diameter in the regularization fit.

The photometer was also used for electrophoretic mobility measurements of pooled and formulated samples of each construct. The samples of different TMPs were pooled and dialyzed into a pH 7.2 buffer of 50 mM Tris and 100 mM sodium chloride. Samples were filtered with a 0.2 μm PES filter (VWR International) and concentration was adjusted with Vivaspin 20 filters with a 30 kDa pore rating (Sartorius). The sample of 50 μm was inserted into buffer-filled folded disposable capillary cells (DTS1070; Malvern Instruments) using a diffusion barrier technique (Patent WO2012083272A1). Samples were measured in pentaplicates in automatic mode. Each measurement comprised a 120 s equilibration and five runs with up to 15 sub runs. The measurements were performed at 60 mV and 25°C. Zeta potential was calculated by Zetasizer Software version 7.12 (Malvern Instruments) assuming a material refractive index of 1.45, absorption of 0.001, a viscosity of 0.8872 mPas, a dielectric constant of 78.54, and a Smoluchowski approximation of 1.5 (Smoluchowski, 1921).

The VLPs were furthermore imaged by transmission electron microscopy (TEM) on a Titan^3 80–300 microscope (FEI Company, Hillsboro, US-OR at 80 kV in bright field mode. For sample preparation, carbon-coated 400-mesh copper grids (Plano GmbH, Wetzlar, DE) were first hydrophilized with a 1% (w/v) alcian blue 8GX (Alfa Aesar, Ward Hill, US-MA) for 2 min and washed five times with ultrapure water. Subsequently, the grids were incubated for 2 min with the 0.2 μm filtered 0.3 g/L to 0.5 g/L VLP solutions. The samples were negatively stained with a 1% (w/v) ammonium molybdate(VI) solution (Acros Organics, Geel, BE) at pH 7.2 for 45 s, washed, and air-dried. VLP diameters were measured with ImageJ 1.52a (NIH, Bethesda, US-MD). TEM images were processed by adjusting contrast and lightness to improve the visibility of the VLP particles using RawTherapee version 5.5 (Gábor Horváth) image processing software.

2.5 | Data acquisition and analysis

During experiments, all integrated sensors communicated with a custom application developed in Matlab (version R2016b; The Mathworks, Natick, US-MA). Next, to starting and stopping measurements, the application gathered the sensor signals (three pressure signals, the permeate weight, *z*-average, and UV/Vis absorbance spectra). Communication and control were performed through software libraries provided by the different instrument software. The signals were displayed on the graphical user interface (GUI) and stored on the hard drive with a time stamp. For calculating the permeate volume, the density of the permeate was assumed to be 1 g/cm^3 Data acquisition and analysis of light scattering and UV/Vis measurements were performed as described below.

2.5.1 | Light scattering measurements

The Zetasizer Nano ZSP was utilized for DLS and SLS measurements using the chromatography flow standard operating orocedure (SOP) of the Zetasizer software (version 7.12; Malvern Instruments). The Zetasizer acquires data in a back-scattering geometry at 173°. Each measurement duration was 10 s. While DLS measurements were exported on-line, SLS data was extracted off-line. From the DLS measurement, the *z*-average was obtained as calculated by the Zetasizer software by the method of cumulants (Koppel, 1972). Viscosity (0.8872 mPas), refractive indices (protein 1.45; water 1.33;

as provided by the Zetasizer software), temperature (25°C), and flow rate (1 ml/min) were assumed to be constant for the calculation of the *z*-average. The *z*-average data was subsequently filtered by a moving median over 60 s to remove outliers. The SLS signal was not filtered. The transition from process Phase I to process Phase II was detected from the scattered light intensity by the CUSUM algorithm (Grigg, Farewell, & Spiegelhalter, 2003; Page, 1954). The transition from process Phase II to process Phase III was set at the global maximum of the scattered light intensity.

2.5.2 | UV/Vis absorption measurements and processing

During VLP assembly, UV/Vis spectra were continuously acquired at 1 Hz in the spectral range from 240 nm to 340 nm with a resolution of 1 nm. To gain information on the local environment of aromatic amino acids, the spectral data was filtered by a moving average over 30 s and the second derivatives were computed with a Savitzky-Golay filter (Savitzky & Golay, 1964) of order 5 with a 9-point window (Ausar et al., 2006; Jiskoot and Crommelin, 2005). An example spectrum with the subsequent data evaluation is shown in Figure S1 in the Supporting Information Material A. The resulting second derivative spectra were interpolated with a cubic spline to a final resolution of 0.01 nm. From the interpolated data, the location of the minimum near 292.5 nm was used as a measure of tryptophan solvent exposure (Jiskoot and Crommelin, 2005; Mach & Middaugh, 1994). The exposure of tyrosine was assessed based on the a/b-ratio as defined by (Ragone, Colonna, Balestrieri, Servillo, & Irace, 1984). Briefly, the vertical distance between trough and peak near 285 nm *a* was normalized by the trough-peak distance near 294 nm *b*. The inflection point of the a/b-ratio over time was computed by taking the first derivative with a second-order Savitzky-Golay filter (window width 501 points corresponding to 8.35 min) and finding the minimum.

2.5.3 | Partial-Least Squares model calibration

Partial-least squares (PLS) model calibration was performed in Matlab (version 2016a). For each VLP, a PLS model was calibrated based on the UV/Vis spectroscopic data in combination with the off-line SEC VLP concentration. Data of all three TMPs were included in one model. PLS model calibration was performed similarly as described previously (Großhans et al., 2018). The data were first preprocessed and subsequently fitted with a PLS-1 model by the SIMPLS algorithm (de Jong, 1993). For preprocessing, a Savitzky-Golay filter with a second-order polynomial was applied on the spectra and, optionally, the first or second derivative was taken. Cross-validation was performed by iteratively excluding one sample of each CFF run ($\frac{1}{7}$ of the data for VLP A and B, $\frac{1}{6}$ of the data for VLP C), calibrating a PLS model on the remaining samples ($\frac{6}{7}$ of the data for VLP A and B, $\frac{5}{6}$ of the data for VLP C), and calculating a residual sum of squares on the excluded run. This procedure was repeated until all runs had been excluded once. All residual sums of squares for the different submodels were subsequently accumulated yielding the predictive residual sum of squares (PRESS). The PRESS was scaled according to Wold et al. (2001) by the number of samples and latent variables used in the PLS model. Based on the scaled PRESS, an optimization was performed using the built-in genetic algorithm of Matlab for integers (Deep, Singh, Kansal, & Mohan, 2009). The genetic algorithm optimized the window width of the Savitzky-Golay filter $5 \leq w \leq 21$, the order of derivative $0 \leq n \leq 2$ as well as the number of latent variables for the PLS-1 model $4 \leq N \leq 14$. The root mean squared error cross validation (RMSECV) was calculated from the PRESS by dividing by the total number of samples. The Q^2 and R^2 values were calculated by dividing the PRESS, respectively the residual sum of squares, by the summed squares of the response corrected to the mean (Wold et al., 2001).

3 | RESULTS

In this study, a new UF/DF setup with an on-line measurement loop was developed to monitor VLP reassembly steps. In the measurement loop, a UV/Vis spectrometer and a light scattering photometer were integrated. Furthermore, an application was implemented in Matlab providing a GUI, communication capabilities to the different sensors as well as a common time base for all performed measurements. This allowed for acquiring and synchronizing measurements in a controlled manner. Within the application, UV/Vis spectra, DLS measurements, pressure, and weight readings were immediately available for processing and display. To demonstrate the advantages of this experimental setup, nine UF/DF runs with three different HBcAg constructs at three different TMPs were performed.

3.1 | Monitoring of standard processes parameters

During the UF/DF processes, the initial buffer was replaced by reassembly buffer to form HBcAg VLPs from homodimers. In Table 1, process data of all runs are summarized (original data presented in Figure S2 in the Supporting Information Material C). The table also shows that the feedstock purity of VLP A was higher than VLP C and VLP B. At 0.25 bar TMP, VLP A, B, and C showed nearly constant increases in permeate mass over time implicating constant fluxes. The average flux for these three runs was 25.8 L/m^{2}h to 29.1 L/m^{2}h. At 0.5 bar and 1 bar TMP, the average flux was higher for all three VLPs (from 36.3 L/m^{2}h to 48.7 L/m^{2}h). CFF processes at 0.5 bar and 1 bar TMP showed a decreasing flux over time after an initial constant phase (except for VLP B at 0.5 bar). A decrease in flux at constant TMP indicates the formation of a fouling layer on the membrane (Huisman, Prádanos, & Hernández, 2000; van den Berg & Smolders, 1990).

3.2 | Process monitoring with on-line PAT sensors

In Figures 4, 5, and 6, the on-line PAT sensor measurements as well as SEC off-line analytics are shown for VLP A, B, and C, respectively. All data were plotted over DV indicating the progress of buffer exchange. Each figure shows the absorbance at 280 nm, off-line VLP

TABLE 1 Process data is summarized for all performed runs

	VLP A			VLP B			VLP C		
TMP/bar	**0.25**	**0.5**	**1**	**0.25**	**0.5**	**1**	**0.25**	**0.5**	**1**
Feedstock purity[a]/%		73.5			22.6			44.1	
Zeta potential[b]/mV		−7.9(7)			−11.8(6)			−9.5(8)	
Total run time/min	118	78	75	133	75	79	108	71	70
Mean flux/(Lm^{-2}h^{-1})	30.5	46.9	48.4	26.8	48.7	45.9	27.6	36.3	40.0
Max. VLP conc./(g/L)	0.248	0.275	0.250	0.126	0.133	0.116	0.134	0.103	0.126
Inflection a/b-ratio/DV	1.5	0.8	0.7	1.5	1.4	0.7	1.6	0.9	0.6
VLP peak diameter[c]/nm	40(6)	46(11)	42(7)	35(5)	40(11)	46(10)	41(12)	48(5)	36(11)

Note. TMP: transmembrane pressure; VLP: Virus-like particle.

[a]Assessed by reversed-phase chromatography as described in the Supporting Information Material B.

[b]Median and median absolute deviation in parenthesis.

[c]Mean and standard deviation of all DLS acquisitions ($n = 36 - 42$) in parenthesis.

concentration measurements by SEC, second derivative spectral analysis, and light scattering data. It is important to note that an insufficient scattered light intensity was recorded for VLP C at 1 bar TMP due to an incorrectly set laser attenuation. The corresponding light scattering results were excluded. The run could not be repeated because of material constraints.

Off-line SEC was performed in triplicates resulting in standard deviations smaller than 0.011 g/L. In all runs, the off-line VLP concentration first remained 0, followed by an increase to the maximum VLP concentration. Thereafter, the concentration was approximately constant or decreased slightly. Depending on the TMP, off-line VLP concentration started to increase at 0.5 DV to 1.5

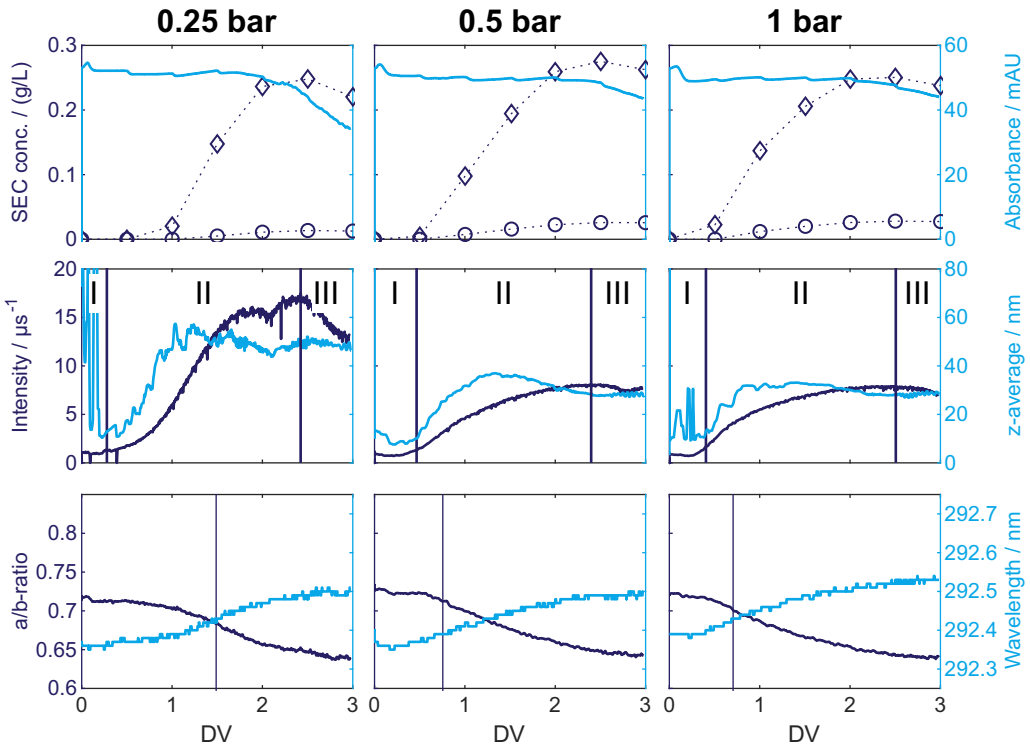

FIGURE 4 The figure displays the on-line sensor measurements as well as off-line analytics against the DV of VLP A. The rows display measurements of different sensors. Top row: Off-line VLP ◇ and aggregate ○ concentration measurements by SEC, UV absorbance at 280 nm –. Middle row: DLS and SLS measurements. Roman numbers indicate the different process phases. Bottom row: Second derivative spectral analysis for tyrosine (a/b-ratio) and tryptophan (location of the minimum around 292.5 nm). The inflection point of the a/b-ratio is marked by a vertical bar. The columns correspond to different TMPs. Left column: 0.25 bar, middle column: 0.5 bar, right column: 1 bar. At 0.25 bar TMP the z-average is corrupted with noise early in the process. DLS: dynamic light scattering; DV: diafiltration volume; SEC: size-exclusion chromatography; SLS: static light scattering; TMP: transmembrane pressure; VLP: virus-like particle [Color figure can be viewed at wileyonlinelibrary.com]

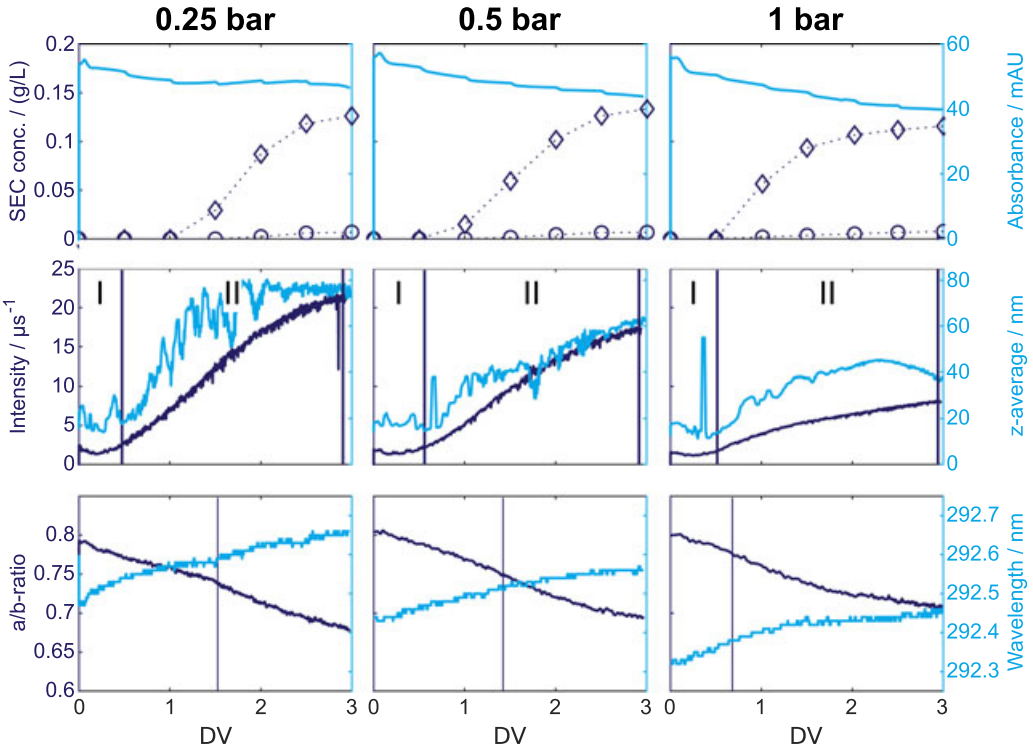

FIGURE 5 The figure displays the on-line sensor measurements as well as off-line analytics against the DV of VLP B. The rows display measurements of different sensors. Top row: Off-line VLP ◇ and aggregate ○ concentration measurements by SEC, UV absorbance at 280 nm – Middle row: DLS and SLS measurements. Roman numbers indicate process phases. Bottom row: Second derivative spectral analysis for tyrosine (a/b-ratio) and tryptophan (location of the minimum around 292.5 nm). The inflection point of the a/b-ratio is marked by a vertical bar. The columns correspond to different TMPs. Left column: 0.25 bar, middle column: 0.5 bar, right column: 1 bar. DLS: dynamic light scattering; DV: diafiltration volume; SEC: size-exclusion chromatography; SLS: static light scattering; TMP: transmembrane pressure; VLP: virus-like particle [Color figure can be viewed at wileyonlinelibrary.com]

DV. The higher the TMP, the lower the DV at which the assembly onset occurred. The maximum observed VLP concentration was between 0.248 g/L and 0.275 g/L for VLP A, between 0.116 g/L and 0.133 g/L for VLP B, and between 0.103 g/L and 0.134 g/L for VLP C. The SEC aggregate content was between 5% and 15% of the VLP concentration.

UV absorbance at 280 nm decreased in all runs over time. Small step-like decreases were due to sampling for off-line analytics. The drawn sample volume was replaced by reassembly buffer resulting in dilution of the process liquid. For VLP A, B, and C, a rapid decrease in the absorbance at 0.25 bar TMP occurred towards the end of the runs, suggesting a loss of protein.

Solvatization of aromatic amino acids and particle formation were observed during CFF by on-line UV/Vis and light scattering measurements. UV/Vis spectral data were examined by second derivative analysis. From the derived spectra, characteristics were calculated for the solvatization of tryptophan (location of the minimum around 292.5 nm) and tyrosine (a/b-ratio; Jiskoot and Crommelin, 2005). For all runs, a shift towards longer wavelengths of the tryptophan minimum was observed, while the a/b-ratio decreased. Both trends indicated an increase in the mean hydrophobicity around tryptophans and tyrosines. Especially for higher TMPs, the characteristics followed a sigmoidal curve shape. The inflection points of the a/b-ratio in all runs were marked by a vertical line and were located either around 0.8 DV or 1.5 DV (see Table 1).

DLS measurements were interpreted based on the *z*-average. In all experiments, an initial phase of relatively constant *z*-average values below 20 nm was observed. The second phase was characterized by a rapid increase in *z*-average to around 40 nm for TMPs of 0.5 bar and 1 bar. At a TMP of 0.25 bar, the second phase showed a larger increase of the *z*-average to 50 nm to 80 nm. The third phase resulted in relatively constant *z*-averages over time.

SLS measurements are influenced by the particle diameter and concentration. Similar to the *z*-average, scattered light intensities started to increase after an initial constant phase. The increase continued even after the *z*-average reached a plateau and eventually flattened. For VLP A and C at 0.25 bar TMP, scattered light intensities rapidly decreased towards the end of the runs.

At 0.5 bar and 1 bar, *z*-averages, scattering intensities, and SEC VLP concentrations of each run started to increase simultaneously within off-line time resolution. Interestingly, for processes at 0.25 bar, the *z*-averages and scattering intensities increased earlier than VLP and aggregate concentration by SEC. The initial increase in Phase II at 0.25 bar ended at high *z*-averages> 45 nm, not observed in the other processes. In all runs, the inflection point of the a/b-ratio occurred around the steepest increase in the VLP concentration by SEC.

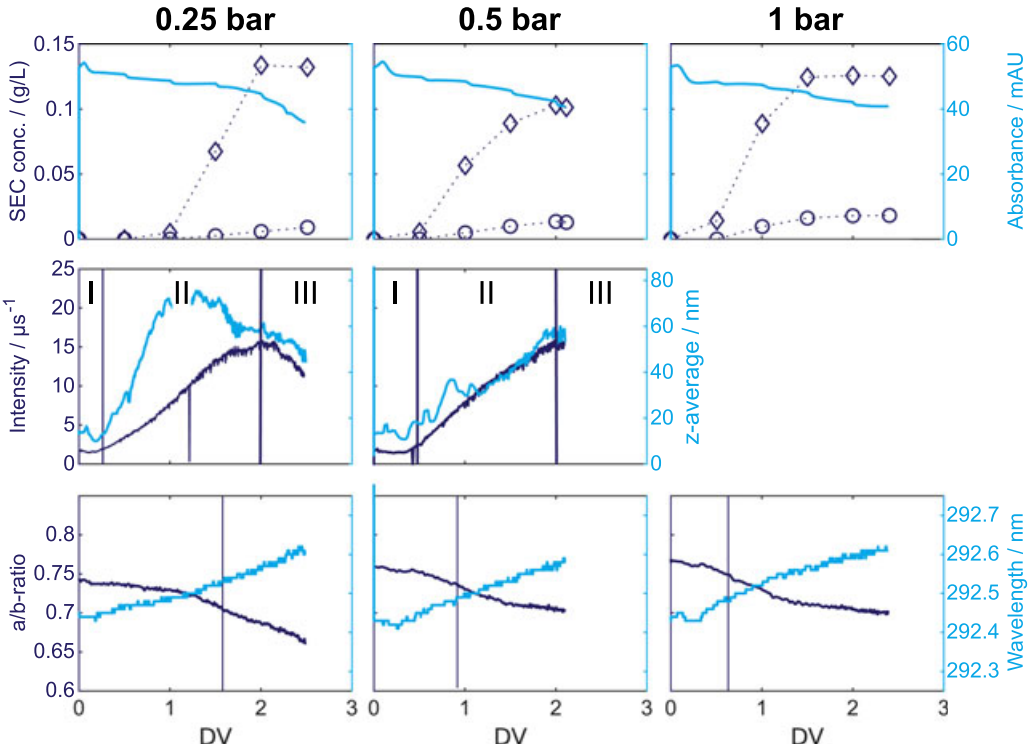

FIGURE 6 The figure displays the on-line sensor measurements as well as off-line analytics against the DV of VLP C. The rows display measurements of different sensors. Top row: Off-line VLP ◇ and aggregate ○ concentration measurements by SEC, UV absorbance at 280 nm –. Middle row: DLS and SLS measurements. Roman numbers indicate process phases. Bottom row: Second derivative spectral analysis for tyrosine (a/b-ratio) and tryptophan (location of the minimum around 292.5 nm). The inflection point of the a/b-ratio is marked by a vertical bar. The columns correspond to different TMPs. Left column: 0.25 bar, middle column: 0.5 bar, right column: 1 bar. DLS and SLS measurements at 1 bar were excluded because of an erratically set laser attenuator. DLS: dynamic light scattering; DV: diafiltration volume; SEC: size-exclusion chromatography; SLS: static light scattering; TMP: transmembrane pressure; VLP: virus-like particle [Color figure can be viewed at wileyonlinelibrary.com]

3.3 | Selective prediction of VLP concentration by PLS modeling

The PLS model calibration results are shown in Figure 7 and Table 2. Figure 8 shows the PLS regression coefficients. All PLS models were fitted to the second derivative of the UV/Vis spectral data with 6–9 latent variables. The achieved Q^2 values were 0.984, 0.984, and 0.947 for VLP A, B, and C, respectively.

3.4 | Analysis of post-assembly samples

Off-line DLS data were measured at the end of all processes. The VLP peak diameter data is shown in Table 1. The mean diameter across all runs was 41 nm with a standard deviation of 11 nm. VLP B had the most negative zeta potential with −11.8(6) mV, followed by VLP C with −9,5(8) mV, and VLP A with −7,9(7) mV.

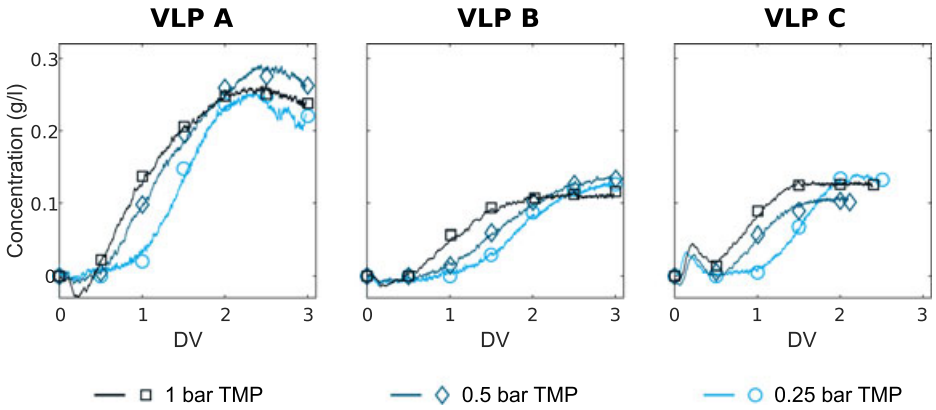

FIGURE 7 A PLS model was fitted to the UV/Vis spectral data for each construct to predict the concentration of assembled VLPs. The concentration estimated by the calibrated PLS model is compared with off-line analytics in the current plot. Each TMP is reflected by a color. The markers show the concentration measured by off-line analytics while the lines correspond to the concentrations estimated by the PLS model. PLS: partial-least squares; TMP: transmembrane pressure; VLP: virus-like particle [Color figure can be viewed at wileyonlinelibrary.com]

TABLE 2 Spectral preprocessing parameters, parameters for the PLS model, and the prediction quality of the chemometric models are summarized

	VLP A	VLP B	VLP C
No. of samples	21	21	18
No. of cross-validation groups	7	7	6
No. of latent variables	6	9	7
Window Savitzky-Golay filter	7	9	9
Derivative	2	2	2
R^2	0.995	0.997	0.994
Q^2	0.984	0.984	0.947
RMSECV/(g/L)	0.01	0.01	0.01

Note. PLS: partial-least squares; RMSECV: root mean squared error cross validation; VLP: virus-like particle.

TEM images (Figure 9) showed hollow spherical particles with a mean diameter of 33(3) nm, 32(2) nm, and 31(2) nm for the formulated and filtered solution of VLPs A, B, and C, respectively. This result is well in agreement with the DLS measurements and literature data (Crowther et al., 1994).

4 | DISCUSSION

4.1 | On-line measurement setup

As shown in Figure 2, the experimental setup included a flow restrictor and a filter next to the sensors in the on-line measurement loop. The flow restrictor and filter were added to improve the measurement quality. The flow restrictor set a minimal back pressure in the measurement loop reducing pressure fluctuations and air bubbles. The filter (cutoff, 0.7 μm) retained bubbles and large particles adversely affecting light scattering measurements. The light scattering measurements depend strongly on the particle diameter d(Bohren & Huffman, 2004). Thus, large particles, such as air bubbles or large aggregates, can completely overshadow the light scattering of smaller particles in SLS and DLS measurements.

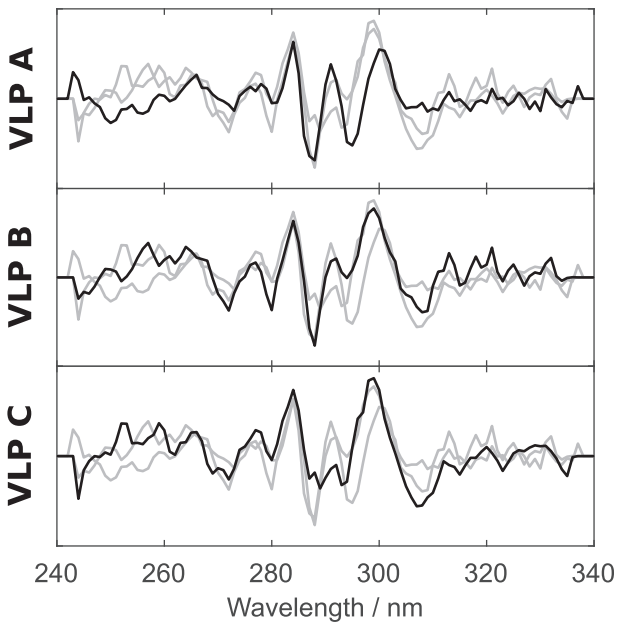

FIGURE 8 Regression coefficients of the three PLS models. Each row corresponds to the regression coefficients of one VLP in black while the other regression coefficients are supplemented in gray. PLS: partial-least squares; VLP: virus-like particle

4.2 | Interpretation of SLS and DLS measurements

During VLP reassembly, anticipated particles in the process solution were homodimers, VLPs, VLP aggregates, and process-related impurities, all of which contributed to light scattering. Thus, the scattered light intensity is a sum signal generated by all scattering species. By neglecting any interaction between the particles and assuming Rayleigh scattering, the scattered light intensity I_R can be described as (Bohren & Huffman, 2004)

$$I_R \propto \sum_i c_i d_i^6, \tag{1}$$

where i iterates overall species, c_i is the molar concentration of species i, and d_i is the diameter of species i. Based on this formula, it can be verified that particle agglomeration and concentration leads to increased scattered light intensities.

The z-average is the intensity-weighted harmonic mean hydrodynamic diameter (Thomas, 1987). Therefore, the z-average is not proportional to the concentration but reflects an apparent mean particle diameter. A small fraction of large particles can still significantly increase the z-average. During reassembly, an increase of scattered light intensity and z-average was expected because of the formation of VLPs and aggregates.

4.3 | DLS measurements inflow

DLS measures the time correlation of scattered light intensity. In contrast to the typical DLS measurement setup, the time correlation in the on-line measurement loop was not only influenced by diffusion but also by convective flow (Berne & Pecora, 2000). It has been previously demonstrated that the convective flow results in increased estimated diffusion coefficients and thus in reduced particle diameters (Leung, Suh, & Ansari, 2006). The effect was shown to be more pronounced for larger particles. Consequently, underestimation of particle sizes was expected to be more pronounced for aggregates than VLPs than homodimers. No effect on SLS was expected from convective flow.

4.4 | General considerations on the VLP assembly processes

During the diafiltration process, the disassembly buffer was gradually exchanged by an assembly buffer. The chemical environment of the HBcAg dimers increasingly favored assembly. This is different to the

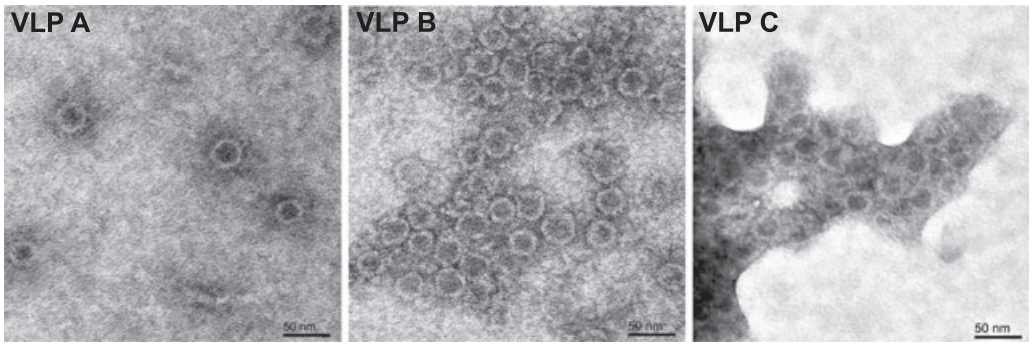

FIGURE 9 TEM micrographs of the formulated VLP A, B, and C after the end of the assembly process by CFF. CFF: cross-flow filtration; TEM: transmission electron microscopy; VLP: virus-like particle

conventional approach in VLP kinetic studies where the composition of the assembly reaction liquid is usually adjusted by rapid dilution (Mukherjee, Thorsteinsson, Johnston, DePhillips, & Zlotnick, 2008; Zlotnick, Johnson, Wingfield, Stahl, & Endres, 1999). In said studies, assembly equilibrium phases were reached in a few minutes. Given the comparably large time frame of diafiltration experiments (75 min–135 min), we assume that the VLP concentration was almost exclusively dependent on the buffer composition.

Figure 10 illustrates the formation of particles out of HBcAg dimers during a diafiltration process and expected sensor responses. The diafiltration process was split into Phases I to III based on different reactions occurring during each phase.

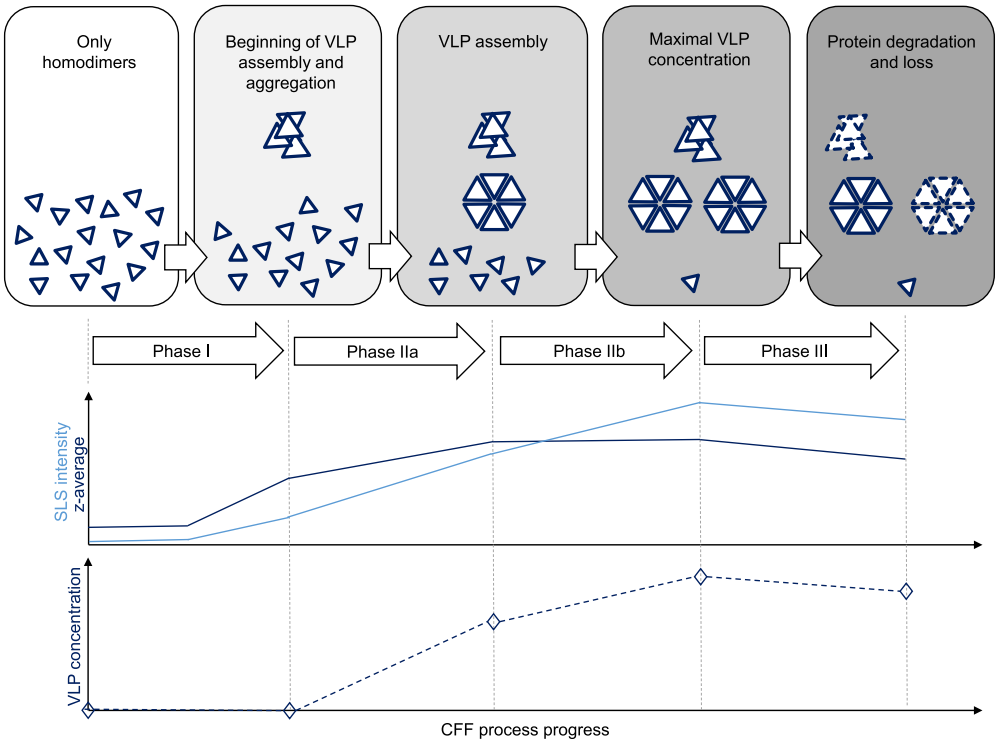

FIGURE 10 Theoretical consideration of particle formation during the assembly process by CFF. Homodimers, aggregates, and VLPs are shown as schematics. The expected development of SLS, *z*-average, and VLP concentration signals is shown over the CFF process progress subdivided into four phases. In the process, the buffer of a homodimer solution is gradually exchanged by assembly buffer to initiate VLP assembly. In Phase I, few aggregates are formed and no assembly takes place. The formation of aggregates increases the light scattering signals while the VLP concentration remains 0. As a consequence of exceeding a critical buffer composition, VLPs start to form in Phase IIa, visualized by an increase in VLP concentration. The light scattering signals continue to increase as a response to particle formation. In Phase IIb, assembly continues, indicated by a further increase in VLP concentration and static light scattering. The *z*-average remains comparably constant as its value is already close to the actual VLP diameter and is thus only marginally influenced by further assembly. In Phase III, the assembly reaction is no longer proceeding. Particles are depleted resulting in a decrease in the light scattering signals. CFF: cross-flow filtration; SLS: static light scattering; VLP: virus-like particle [Color figure can be viewed at wileyonlinelibrary.com]

In Phase I, buffer exchange starts but no assembly occurs, i.e., the VLP concentration remains 0. However, aggregates may form resulting in an increase in scattered light intensity and *z*-average, as seen in Figures 4, 5, and 6.

In Phase II, homodimers assemble into VLPs. Native HBcAg VLPs are 30 nm to 34 nm in diameter (Crowther et al., 1994). VLP concentration increases to its maximum, while the scattered light intensity and *z*-average continue to rise. To explain the sensor response more comprehensively, Phase II was subdivided into two subphases, IIa and IIb. In subphase IIa, *z*-average and scattered light intensity both increase. In subphase IIb, scattered light intensity further increases while *z*-average remains constant. The increase in scattered light intensity is caused by the ongoing formation of VLPs and aggregates. Conversely, the *z*-average stagnates as it is an intensity-weighted harmonic mean. Native HBcAg VLPs are 30 nm to 34 nm in diameter (Crowther et al., 1994). When the *z*-average is close to the size of VLPs, further assembly has only a small effect on the *z*-average, while the scattered light intensity still increases due to the formation of particles.

In Phase III, the VLP concentration no longer increases. Thus, the end of the assembly process is reached. A loss of aggregates is reflected by a decrease in *z*-average and scattered light intensity. A decrease in scattered light intensity and UV absorbance with constant *z*-average reflects a decrease in overall protein concentration with constant particle size distribution.

Towards the end of some processes (most pronounced for VLP A and C at 0.25 bar), both light scattering signals decreased combined with a decrease in the UV signal at 280 nm. Thus, the protein concentration decreased due to adsorption to the CFF membrane or retention on the measurement loop filter. The elevated salt concentration of the process liquid at this stage of the process may have promoted adsorption of protein to the hollow fiber membrane (Hanemaaijer et al., 1989). In both runs, the *z*-average started to decrease already earlier than the UV signal at 280 nm around the location of the inflection point of the a/b-ratio while the UV absorbance was still approximately constant. This could indicate a partial disintegration of aggregates. Phase III was generally short, as either its onset was close to the final DV or the process was stopped early due to membrane fouling.

The assembly of HBcAc VLPs also induces changes in mean hydrophobicity around aromatic amino acids as capsid assembly relies on hydrophobic interaction forces (Venkatakrishnan & Zlotnick, 2016; Wynne et al., 1999). Tyrosine-132 is especially important for the assembly (Bourne, Katen, Fulz, Packianathan, & Zlotnick, 2009). In homodimers, tyrosine-132 is highly solvent-exposed, as shown in Figure 3. After VLP assembly, tyrosine-132 is buried in a hydrophobic pocket of the neighboring homodimer. During diafiltration, the solvatization of tyrosine changes because of aggregation as well as VLP assembly. If the mean effect on hydrophobicity by aggregation is small compared to the mean effect caused by assembly, the change over time of the a/b-ratio correlates to the rate of assembly. As a result, the a/b-ratio's inflection point marks the point of the highest rate of assembly. Similarly, the increase in the wavelength of the tryptophan absorption minimum marks an increase in hydrophobicity around tryptophans. Since the change in the solvent exposure of tryptophans during VLP assembly is less pronounced, the effect is weaker and more biased by aggregation.

4.5 | CFF for VLP assembly

VLP A was assembled from the purest dimer stock solution of the three investigated VLPs. The process was thus expected to perform comparably well. This agreed with the experimental results at 0.5 bar and 1 bar TMP. The observed *z*-averages of 28 nm to 29 nm in Phase III showed that there was a significant fraction of VLPs. Few large particles were generated while other factors such as the flow reduced the *z*-average compared with off-line DLS analytics (see Table 1). The higher final *z*-average and an elevated scattered light intensity at 0.25 bar TMP provided evidence of the formation of large aggregates. The observations made for VLP A were in general also applicable to VLP B and C. Both VLPs were adversely affected at lower TMPs by aggregation reflected by increased *z*-averages and light scattering intensities.

A further interesting result of this study was the clustering of the inflection points of the a/b-ratio either around 1.5 DV or around 0.8 DV. An early inflection point is consistent with early VLP formation. Conversely, a late inflection point correlated to an early increase in aggregates. By keeping in mind that the DV is indicative of the progress of buffer exchange, the conclusion may be drawn that VLP assembly is inhibited by aggregates. Indeed, a similar conclusion was previously proposed for MuPyVP1 VLPs (Ding, Chuan, He, & Middelberg, 2010). Ding and coworkers described a competition of capsomere association into aggregates and precursors of MuPyVP1 VLPs.

The results of the diafiltration experiments for all VLPs showed that a low TMP of 0.25 bar lead to an increased aggregation propensity and an increased process time compared with the other conditions. At 0.5 bar and 1 bar TMP, the process time, VLP concentration, and aggregate content depended on the VLP construct and stock purity but were not solely dependent on the TMP. For increased yield and decreased aggregate content, it could be helpful to introduce a further purification step for VLP B and C. In all runs, aggregate concentration by SEC did not reflect the data obtained by light scattering. The reason for this seemed to be that large aggregates were depleted during sample preparation or in the SEC column. As a consequence, light scattering provided a more complete picture of the aggregate content.

Process Phase III is characterized by product loss. The process should therefore be terminated at the end of Phase II. It is worth noting that the end of Phase II is influenced by the VLP construct but seems to be independent of the applied TMP. No plateau or decrease in assembly was observed for VLP B. VLP B was charged strongest, requiring higher ionic strengths to overcome the electrostatic charges of the homodimers during assembly (see Table 1). Zeta potentials of VLP A and C are similar. For both, a transition into Phase III was observed.

To compare the assembled VLPs with standard characterization methods, we performed DLS and TEM measurements on the assembled VLPs. Off-line DLS VLP peak diameters with a mean of 41 nm and a standard deviation of 11 nm are comparable with that of wild type HBcAg VLPs (typically 30 nm to 34 nm (Crowther et al., 1994). No significant influence of the TMP or construct on the final VLP peak diameter could be observed. TEM measurements confirmed the existence of assembled VLPs for all three constructs in the expected size range.

In summary, the analytical measurements of the VLP size and structure confirm the information obtained from the PAT tools.

4.6 | Benefits of using PAT for process development and production

PAT is currently a frequently investigated approach to increasing the acquired information about unit operations in biopharmaceutical process development and production by timely measurements. Generating information on the process in (near) real-time potentially results in a better understanding, faster optimization, and reduced off-line analytical samples (Bakeev, 2010).

Here, the UV absorbance at 280 nm provided insight into changes in the concentration of protein and other absorbing species in real time. This can be of advantage for assessing the membrane performance (e.g., membrane fouling, pore rating out-of-specification, or membrane damage). A mechanistic understanding is, however, often not possible solely based on a single wavelength. A more in-depth view on the ongoing processes during UF/DF could be realized based on the acquired UV/Vis spectra. For HBcAg, tyrosine-132 is especially important for the VLP assembly. The a/b-ratio provides a mechanistic insight into the assembly reaction based on the mean tyrosine solvatization. Next to means for quantification, the UV/Vis spectrometer implemented in the presented setup thus provides mechanistic process understanding. Furthermore, other UV/Vis chromophores are phenylalanine, tryptophan, and disulfide bridges (Jiskoot and Crommelin, 2005). These may be affected during the assembly of other VLPs. For example, during the assembly of human papilloma virus-like particles, disulfide bridges are the key to the formation of higher order structures (Li, Beard, Estes, Lyon, & Garcea, 1998). An assembly process with these VLPs could therefore be monitored with a UV/Vis spectrometer.

Another changing protein attribute which can be monitored is the particle size. The significant increase in size has a large impact on the scattering characteristics of the process fluid. The light scattering photometer thus allowed for the detection of the start of the assembly reaction and maximum VLP concentration. Light scattering photometers are universal detectors that are not dependent on the protein primary structure. As a consequence, any VLP assembly reaction can be monitored with this technique. In development and production, light scattering detectors provide the means for detecting the ideal point to stop CFF or to initiate the next process step. This can improve the product quality (as process Phase III is omitted) and allow for process intensification.

Generally, the on-line sensors provide data with high temporal resolution which typically is difficult to achieve with off-line analytics. In consequence, smaller changes in process characteristics (e.g., assembly onset, end of Phase II) can be detected. This may be helpful for the further assessment of different processes in development or for detecting deviations or hidden trends in production.

For process monitoring in production, it may be beneficial to retrieve VLP concentrations in real time. A PLS model was thus developed to demonstrate the possibility to monitor VLP concentration on-line by UV/Vis spectroscopy. The model was optimized by a constrained heuristic search algorithm. The minimal number of four latent variables was set to reflect the minimal amount of independent UV-active species (VLP concentration, deoxyribonucleic acid (DNA) concentration, urea concentration, and aggregates). Reliable VLP concentration estimations were possible for all three constructs. In production, UV/Vis measurements in conjunction with a PLS model could thus be used for the real-time assessment of the assembly progress and ultimately for process control. Based on the regression coefficients of the PLS model (Figure 8), it is clearly visible that the fine structure of the tyrosine and tryptophan absorption is of major importance for the regression. Therefore, the PLS model accesses information similar to that provided by the a/b-ratio and the tryptophan minimum. The differences between the regression coefficients for VLP A, B, and C were attributed to the changing purity of the stock solutions. Provided that no additional chromophores are introduced into the MIR, a universally applicable PLS model for different HBcAg constructs is conceivable. This may be evaluated further in future studies.

5 | CONCLUSION AND OUTLOOK

In this study, we investigated HBcAg assembly by diafiltration of three different constructs at three different TMPs. We developed an on-line measurement setup consisting of a UV/Vis and a light scattering sensor (DLS and SLS) with a unified software platform. This setup allowed for monitoring mean particle sizes, hydrophobicity around tyrosine and tryptophan as well as the protein concentration. VLP particle formation was verified by off-line DLS measurements and TEM imaging. Based on the acquired UV/Vis spectra, we calibrated three PLS models for estimating VLP concentrations in real-time. Regarding process performance, we observed that processes with hollow fiber modules at 0.25 bar TMP resulted in increased aggregation. In all processes, the maximum rate of assembly occurred around two characteristic DV. This behavior was interpreted as a result of aggregation-related inhibition of VLP assembly, which makes it especially important to prevent aggregation in a VLP assembly process. The maximum VLP concentration coincided with the maximum light scattering intensity. Thus, the light scattering peak or the calibrated PLS model could potentially be used as PAT decision tools for VLP assembly process control leading to improved product quality and intensified processes. In summary, the established setup has shown great potential for improving

process monitoring, development, and understanding during VLP assembly by diafiltration.

In the future, strategies may have to be developed for process control during VLP reassembly. The proposed setup allowed for monitoring central quality attributes during the process with and without calibrated chemometric models. It is therefore a good starting point for any further research in this direction. From a process development point of view, the current results have not yet shown a reduced process efficiency at the highest TMP. A further increase in TMP may thus be attractive. Alternative membrane options, such as membrane cassettes, could strongly affect the process and may be interesting to evaluate with the setup.

ACKNOWLEDGMENTS

This project received funding from Deutsche Forschungsgemeinschaft (DFG) in the frame of SPP 1934, Project number 273937032. The authors thank BioNTech Protein Therapeutics GmbH for providing the VLP constructs and the production process scheme, especially Anja Wilming, Thomas Hiller, and Thorsten Klamp for their collaboration. The authors express their gratitude to Reinhard Schneider for technical and scientific support in preparing and performing TEM imaging. The authors are thankful for the thorough review of the manuscript by Dr.-Ing. Josefine Morgenstern, Laura Rolinger, and Heidemarie Knieriem.

ORCID

Matthias Rüdt http://orcid.org/0000-0002-8583-6645
Philipp Vormittag http://orcid.org/0000-0002-5663-2168
Jürgen Hubbuch http://orcid.org/0000-0003-0839-561X

REFERENCES

Alexander, C. G., Jürgens, M. C., Shepherd, D. A., Freund, S. M. V., Ashcroft, A. E., & Ferguson, N. (2013). Thermodynamic origins of protein folding, allostery, and capsid formation in the human hepatitis b virus core protein. *Proceedings of the National Academy of Sciences*, *110*, E2782–E2791. http://www.pnas.org/content/110/30/E2782.full.pdf

Arora, U., Tyagi, P., Swaminathan, S., & Khanna, N. (2012). Chimeric hepatitis b core antigen virus-like particles displaying the envelope domain iii of dengue virus type 2. *Journal of Nanobiotechnology*, *10*, 30.

Ausar, S. F., Foubert, T. R., Hudson, M. H., Vedvick, T. S., & Middaugh, C. R. (2006). Conformational stability and disassembly of Norwalk virus-like particles: Effect of pH and temperature. *Journal of Biological Chemistry*, *281*, 19478–19488.

Bachmann, M. F., & Whitehead, P. (2013). Active immunotherapy for chronic diseases. *Vaccine*, *31*, 1777–1784.

Bakeev, K. A. (2010). *Process Analytical Technology: Spectroscopic Tools and Implementation Strategies for the Chemical and Pharmaceutical Industries* (2nd ed.). Chichester, GB-WSX: John Wiley & Sons.

van den Berg, G., & Smolders, C. (1990). Flux decline in ultrafiltration processes. *Desalination*, *77*, 101–133.

Berne, B. J., & Pecora, R. (2000). *Dynamic Light Scattering: With Applications to Chemistry, Biology, and Physics*. Mineola, US-NY: Dover Publications.

Bohren, C. F., & Huffman, D. R. (2004). *Absorption and Scattering of Light by Small Particles*. Weinheim, DE: Wiley-VCH.

Bourne, C. R., Katen, S. P., Fulz, M. R., Packianathan, C., & Zlotnick, A. (2009). A mutant hepatitis b virus core protein mimics inhibitors of icosahedral capsid self-assembly. *Biochemistry (Moscow)*, *48*, 1736–1742.

Chuan, Y. P., Wibowo, N., Lua, L. H., & Middelberg, A. P. (2014). The economics of virus-like particle and capsomere vaccines. *Biochemical Engineering Journal*, *90*, 255–263.

Crowther, R., Kiselev, N., Böttcher, B., Berriman, J., Borisova, G., Ose, V., & Pumpens, P. (1994). Three-dimensional structure of hepatitis b virus core particles determined by electron cryomicroscopy. *Cell*, *77*, 943–950.

Deep, K., Singh, K. P., Kansal, M., & Mohan, C. (2009). A real coded genetic algorithm for solving integer and mixed integer optimization problems. *Applied Mathematics and Computation*, *212*, 505–518.

Ding, Y., Chuan, Y. P., He, L., & Middelberg, A. P. (2010). Modeling the competition between aggregation and self-assembly during virus-like particle processing. *Biotechnology and Bioengineering*, *107*, 550–560.

Fang, M., Diao, W., Dong, B., Wei, H., Liu, J., Hua, L., & Wan, M. (2016). Detection of the assembly and disassembly of PCV2b virus-like particles using fluorescence spectroscopy analysis. *Intervirology*, *58*, 318–323.

Gasteiger, E., Hoogland, C., Gattiker, A., Wilkins, M. R., Appel, R. D., Bairoch, A., & Duvaud, S. (2005). Protein identification and analysis tools on the expasy server. In J. M. Walker (Ed.), *The Proteomics Protocols Handbook* (pp. 571–607). Springer.

Grigg, O. A., Farewell, V. T., & Spiegelhalter, D. J. (2003). Use of risk-adjusted CUSUM and RSPRTcharts for monitoring in medical contexts. *Statistical Methods in Medical Research*, *12*, 147–170.

Großhans, S., Rüdt, M., Sanden, A., Brestrich, N., Morgenstern, J., Heissler, S., & Hubbuch, J. (2018). In-line Fourier-transform infrared spectroscopy as a versatile process analytical technology for preparative protein chromatography. *Journal of Chromatography A*, *1547*, 37–44.

Hanemaaijer, J., Robbertsen, T., van den Boomgaard, T., & Gunnink, J. (1989). Fouling of ultrafiltration membranes. The role of protein adsorption and salt precipitation. *Journal of Membrane Science*, *40*, 199–217.

Hanslip, S. J., Zaccai, N. R., Middelberg, A. P., & Falconer, R. J. (2006). Assembly of human papillomavirus type-16 virus-like particles: Multifactorial study of assembly and competing aggregation. *Biotechnology Progress*, *22*, 554–560.

Hu, L., Trefethen, J. M., Zeng, Y., Yee, L., Ohtake, S., Lechuga-Ballesteros, D., & Middaugh, C. R. (2011). Biophysical characterization and conformational stability of Ebola and Marburg virus-like particles. *Journal of Pharmaceutical Sciences*, *100*, 5156–5173.

Huisman, I. H., Prádanos, P., & Hernández, A. (2000). The effect of protein-protein and protein-membrane interactions on membrane fouling in ultrafiltration. *Journal of Membrane Science*, *179*, 79–90.

2005). W. Jiskoot, & D. Crommelin (Eds.), *Methods for Structural Analysis of Protein Pharmaceuticals*. Arlington, US-VA: American Association of Pharmaceutical Scientists.

de Jong, S. (1993). SIMPLS: An alternative approach to partial least squares regression. *Chemometrics and Intelligent Laboratory Systems*, *18*, 251–263.

2008). M. J. Jornitz, M. W. Jornitz, & T. H. Meltzer (Eds.), *Filtration and Purification in the Biopharmaceutical Industry* (2nd ed). Boca Raton, US-FL: CRC Press.

Kaslow, D. C., & Biernaux, S. (2015). RTS,S: Toward a first landmark on the malaria vaccine technology roadmap. *Vaccine*, *33*(52), 7425–7432.

Klamp, T., Schumacher, J., Huber, G., Kühne, C., Meissner, U., Selmi, A., & Sahin, U. (2011). Highly specific auto-antibodies against claudin-18 isoform 2 induced by a chimeric HBcAg virus-like particle vaccine kill tumor cells and inhibit the growth of lung metastases. *Cancer Research*, *71*, 516–527.

Ko, M. K., Pellegrino, J. J., Nassimbene, R., & Marko, P. (1993). Characterization of the adsorption-fouling layer using globular proteins on ultrafiltration membranes. *Journal of Membrane Science*, *76*, 101–120.

Koppel, D. E. (1972). Analysis of macromolecular polydispersity in intensity correlation spectroscopy: The method of cumulants. *The Journal of Chemical Physics*, *57*(11), 4814–4820.

Kumru, O. S., Joshi, S. B., Smith, D. E., Middaugh, C. R., Prusik, T., & Volkin, D. B. (2014). Vaccine instability in the cold chain: Mechanisms, analysis and formulation strategies. *Biologicals*, *42*, 237–259.

Kurnik, R. T., Yu, A. W., Blank, G. S., Burton, A. R., Smith, D., Athalye, A. M., & Van Reis, R. (1995). Buffer exchange using size exclusion chromatography, countercurrent dialysis, and tangential flow filtration: Models, development, and industrial application. *Biotechnology and Bioengineering*, *45*, 149–157.

Kushnir, N., Streatfield, S. J., & Yusibov, V. (2012). Virus-like particles as a highly efficient vaccine platform: Diversity of targets and production systems and advances in clinical development. *Vaccine*, *31*, 58–83.

Ladd Effio, C., & Hubbuch, J. (2015). Next generation vaccines and vectors: Designing downstream processes for recombinant protein-based virus-like particles. *Biotechnology Journal*, *10*, 715–727.

Leung, A. B., Suh, K. I., & Ansari, R. R. (2006). Particle-size and velocity measurements in flowing conditions using dynamic light scattering. *Applied Optics*, *45*, 2186–2190.

Li, M., Beard, P., Estes, P. A., Lyon, M. K., & Garcea, R. L. (1998). Intercapsomeric disulfide bonds in papillomavirus assembly and disassembly. *Journal of Virology*, *72*, 2160–2167. https://jvi.asm.org/content/72/3/2160.full.pdf

Liew, M. W., Chuan, Y. P., & Middelberg, A. P. (2012). Reactive diafiltration for assembly and formulation of virus-like particles. *Biochemical Engineering Journal*, *68*, 120–128.

Link, A., Zabel, F, Schnetzler, Y., Titz, A., Brombacher, F., & Bachmann, M. F. (2012). Innate immunity mediates follicular transport of particulate but not soluble protein antigen. *The Journal of Immunology*, *188*, 3724–3733.

Low, J. G., Lee, L. S., Ooi, E. E., Ethirajulu, K., Yeo, P., Matter, A., & Novotny-Diermayr, V. (2014). Safety and immunogenicity of a virus-like particle pandemic influenza A (H1N1) 2009 vaccine: Results from a double-blinded, randomized Phase I clinical trial in healthy Asian volunteers. *Vaccine*, *32*, 5041–5048.

Lua, L. H., Connors, N. K., Sainsbury, F., Chuan, Y. P., Wibowo, N., & Middelberg, A. P. (2014). Bioengineering virus-like particles as vaccines. *Biotechnology and Bioengineering*, *111*, 425–440.

Mach, H., & Middaugh, C. R. (1994). Simultaneous monitoring of the environment of tryptophan, tyrosine, and phenylalanine residues in proteins by near-ultraviolet second-derivative spectroscopy. *Analytical Biochemistry*, *222*(2), 323–331.

Mach, H., Volkin, D. B., Troutman, R. D., Wang, B., Luo, Z., Jansen, K. U., & Shi, L. (2006). Disassembly and reassembly of yeast-derived recombinant human papillomavirus virus-like particles (HPV VLPs). *Journal of Pharmaceutical Sciences*, *95*, 2195–2206.

Middelberg, A. P., Rivera-Hernandez, T., Wibowo, N., Lua, L. H., Fan, Y., Magor, G., & Batzloff, M. R. (2011). A microbial platform for rapid and low-cost virus-like particle and capsomere vaccines. *Vaccine*, *29*, 7154–7162.

Mukherjee, S., Thorsteinsson, M. V., Johnston, L. B., DePhillips, P. A., & Zlotnick, A. (2008). A quantitative description of in vitro assembly of human papillomavirus 16 virus-like particles. *Journal of Molecular Biology*, *381*, 229–237.

Page, E. S. (1954). Continuous inspection schemes. *Biometrika*, *41*, 100–115.

Peixoto, C., Sousa, M. F. Q., Silva, A. C., Carrondo, M. J. T., & Alves, P. M. (2007). Downstream processing of triple layered rotavirus like particles. *Journal of Biotechnology*, *127*, 452–461.

Ragone, R., Colonna, G., Balestrieri, C., Servillo, L., & Irace, G. (1984). Determination of tyrosine exposure in proteins by second-derivative spectroscopy. *Biochemistry (Moscow)*, *23*, 1871–1875.

Rajendar, B., Sivakumar, V., Sriraman, R., Raheem, M., Lingala, R., & Matur, R. V. (2013). A simple and rapid method to monitor the disassembly and reassembly of virus-like particles. *Analytical Biochemistry*, *440*, 15–17.

Ren, Y., Wong, S. M., & Lim, L. Y. (2006). In vitro-reassembled plant virus-like particles for loading of polyacids. *Journal of General Virology*, *87*, 2749–2754.

Roch, P., & Mandenius, C. F. (2016). On-line monitoring of downstream bioprocesses. *Current Opinion in Chemical Engineering*, *14*, 112–120.

Rüdt, M., Briskot, T., & Hubbuch, J. (2017). Advances in downstream processing of biologics – spectroscopy: An emerging process analytical technology. *Journal of Chromatography A*, *1490*, 2–9.

Russell, B. J., Velez, J. O., Laven, J. J., Johnson, A. J., Chang, G. J. J., & Johnson, B. W. (2007). A comparison of concentration methods applied to non-infectious flavivirus recombinant antigens for use in diagnostic serological assays. *Journal of Virological Methods*, *145*, 62–70.

Savitzky, A., & Golay, M. J. E. (1964). Smoothing and differentiation of data by simplified least squares procedures. *Analytical Chemistry*, *36*, 1627–1639.

Smoluchowski, M. (1921). *Handbuch der Elektrizität und des Magnetismus* (2*). Barth, Leipzig: Stationäre Ströme.*

Thomas, J. C. (1987). The determination of log normal particle size distributions by dynamic light scattering. *Journal of Colloid and Interface Science*, *117*, 187–192.

Venkatakrishnan, B., & Zlotnick, A. (2016). The structural biology of hepatitis B virus: Form and function. *Annual Review of Virology*, *3*, 429–451.

Vicente, T., Burri, S., Wellnitz, S., Walsh, K., Rothe, S., & Liderfelt, J. (2014). Fully aseptic single-use cross flow filtration system for clarification and concentration of cytomegalovirus-like particles. *Engineering in Life Sciences*, *14*, 318–326.

Vicente, T., Roldão, A., Peixoto, C., Carrondo, M. J. T., & Alves, P. M. (2011). Large-scale production and purification of VLP-based vaccines. *Journal of Invertebrate Pathology*, *107*, S42–S48.

Whitacre, D. C., Lee, B. O., & Milich, D. R. (2009). Use of hepadnavirus core proteins as vaccine platforms. *Expert Review of Vaccines*, *8*(11), 1565–1573.

Wold, S., Sjöström, M., & Eriksson, L. (2001). PLS-regression: A basic tool of chemometrics. *Chemometrics and Intelligent Laboratory Systems*, *58*, 109–130.

Wynne, S., Crowther, R., & Leslie, A. (1999). The crystal structure of the human hepatitis B virus capsid. *Molecular Cell*, *3*, 771–780.

Zhao, Q., Allen, M. J., Wang, Y., Wang, B., Wang, N., Shi, L., & Sitrin, R. D. (2012). Disassembly and reassembly improves morphology and thermal stability of human papillomavirus type 16 virus-like particles. *Nanomedicine: Nanotechnology, Biology, and Medicine*, *8*, 1182–1189.

Zhao, Q., Modis, Y., High, K., Towne, V., Meng, Y., Wang, Y., & Sitrin, R. D. (2012). Disassembly and reassembly of human papillomavirus virus-like particles produces more virion-like antibody reactivity. *Journal of Virology*, *9*, 52.

Zlotnick, A., Johnson, J. M., Wingfield, P. W., Stahl, S. J., & Endres, D. (1999). A theoretical model successfully identifies features of hepatitis B virus capsid assembly. *Biochemistry (Moscow)*, *38*, 14644–14652.

SUPPORTING INFORMATION

Additional supporting information may be found online in the Supporting Information section at the end of the article.

How to cite this article: Rüdt M, Vormittag P, Hillebrandt N, Hubbuch J. Process monitoring of virus-like particle reassembly by diafiltration with UV/Vis spectroscopy and light scattering. *Biotechnology and Bioengineering*. 2019;116: 1366–1379. https://doi.org/10.1002/bit.26935